

Graphical Abstract

Oxyfluoride glasses obtained through incorporation of CaF_2 into photovoltaic cover glass melts

Rafaela Valcarenghi, Brenno Greatti Silva, Robson Ferrari Muniz, Vitor Santaella Zanuto, Anna Paulla Simon, Ricardo Schneider, Raquel Dosciatti Bini, Márcio Antônio Fiori, Maxence Vigier, Emmanuel Veron, Mathieu Allix, Marcelo Sandrini, Marcos Paulo Belançon

Highlights

Oxyfluoride glasses obtained through incorporation of CaF_2 into photovoltaic cover glass melts

Rafaela Valcarenghi, Brenno Greatti Silva, Robson Ferrari Muniz, Vitor Santaella Zanuto, Anna Paulla Simon, Ricardo Schneider, Raquel Dosciatti Bini, Márcio Antônio Fiori, Maxence Vigier, Emmanuel Veron, Mathieu Allix, Marcelo Sandrini, Marcos Paulo Belançon

- Glasses containing up to 80% cover glass content were obtained
- Analyses have shown that introducing CaF_2 depolymerizes the material
- These oxyfluoride glasses can be crystallized in several different crystalline phases
- The samples exhibit transparency and thermal stability suitable for optical applications

Oxyfluoride glasses obtained through incorporation of CaF_2 into photovoltaic cover glass melts

Rafaela Valcarenghi^a, Brenno Greatti Silva^b, Robson Ferrari Muniz^b, Vitor Santaella Zanuto^b, Anna Paulla Simon^a, Ricardo Schneider^c, Raquel Dosciatti Bini^a, Márcio Antônio Fiori^{a,d}, Maxence Vigier^e, Emmanuel Veron^e, Mathieu Allix^e, Marcelo Sandrini^a, Marcos Paulo Belançon^a

^a*Universidade Tecnológica Federal do Paraná, Via do Conhecimento Km 01, Pato Branco, 85503-390, Paraná, Brasil*

^b*Universidade Estadual de Maringá, Maringá, , Paraná, Brasil*

^c*Universidade Tecnológica Federal do Paraná, Toledo, Paraná, Brasil*

^d*Universidade da Região de Chapecó, Chapecó, Santa Catarina, Brasil*

^e*Laboratoire CEMHTI, UPR 3079-CNRS, Orléans, France*

Abstract

The glass industry has limited options to mitigate its environmental footprint, and the demand for cover glass to produce photovoltaic panels is increasing. Currently, the majority of this special type of glass is not being recycled, and in this work, we propose to reuse it as raw material to obtain oxyfluoride glasses. The incorporation of CaF_2 and the increasing Na_2CO_3 content resulted in a melting temperature of about 1200°C , significantly lower than in soda-lime glasses, which adds up to the environmental benefits of reusing end-of-life cover glass. The obtained samples show high transparency and thermal stability, allowing the cover glass to make up to 80% of its weight. XRF analysis was employed to determine the elemental composition of the samples, while XRD and Raman indicated that by adding CaF_2 , the glass network was depolymerized. In situ XRD as a function of temperature showed the formation of a few crystalline phases in these oxyfluoride samples, evidencing that it can be explored as a matrix to obtain different glass-ceramics. The combination of the glass properties indicates that this method and the resulting material can contribute to reducing the environmental impact of the glass industry, by creating new glass or glass-ceramic materials that can be obtained at a reduced temperature compared to the soda-lime glass, while cover glass being the primary raw material could reduce the need to extract minerals from nature.

Keywords: cover glass, glass waste management, glass recycling, waste reduction, glass-ceramics, silicate, oxyfluoride

1. Introduction

The world consumes over 130 million tons of glass annually, or about 16 kg per capita. Container and flat glass account for about 80% of global glass production and are estimated to release over 60 million tons of carbon dioxide into the atmosphere, primarily due to the energy-intensive heating of raw materials [1, 2]. Soda-lime is the most common glass, and the industry has limited options to mitigate its environmental footprint. To produce 1 kg of soda-lime glass, the carbonates present in the raw materials will emit around 0.15 kg of CO₂, while the huge amount of energy required to heat and melt ($\sim 1500^\circ\text{C}$) the glass results in another 0.45 kg, primarily due to the combustion of fossil fuels [1, 3]. Even though clean electricity and hydrogen can be employed, these alternatives are yet to be demonstrated at an industrial scale [2, 4].

Though glass can be indefinitely recycled, doing so is often not feasible or attractive due to technical and economic reasons [5, 6]. As discussed in our previous work [7], highly transparent soda-lime is used as cover glasses (CG) in solar energy applications, and these high-quality materials are facing the risk of being dumped in landfills once their demand keeps rising while the options to reuse them are pretty limited. Additionally, glass production requires vast amounts of raw materials, and mining is one of the most energy-intensive industries [8], resulting in a severe environmental impact. These factors highlight the importance of reusing and recycling the CG, turning end-of-life (EOL) products into raw materials to keep them in the market, in a context of circular economy [9, 10, 11].

Glasses other than soda-lime have been proposed as alternatives for solar energy applications, which could include new features such as spectral conversion to enhance Silicon solar panel technology [7]. However, among dozens of proposed glass systems, silicates are the only ones based on abundant, affordable, and non-toxic minerals. The resulting glasses often exhibit high transparency and adequate chemical and mechanical resistance for solar energy applications. Reviewing the literature recently [7, 12], we concluded that modified soda-lime silicates are the most promising system that could meet the requirements needed for mass-scale industrial production, while providing new or enhanced properties that could reduce the industry's energy

consumption, expand solar power production, and contribute significantly to sustainability goals.

An interesting silicate system we have already investigated is achieved when CaF_2 is added into silica melts [13, 14]. While modifiers such as CaO and Na_2O are well-known for reducing the melting temperature of silicates, the F provided from CaF_2 often replaces O, affecting the silica network [15]. Several studies have shown that CaF_2 incorporation reduces the melting temperature and viscosity of silicates [15], while it can improve the microstructure [16] and promote or inhibit the formation of crystalline phases [17, 18], including nanocrystals [19].

To tackle all the above-mentioned questions, this work proposes using CGs from EOL solar panels as raw materials for producing oxyfluoride sodium calcium silicate glasses, achieved through incorporating CaF_2 . Our methodology is simple; the obtained samples have high-optical quality and allow a recycled fraction of raw materials as high as 80% of the final weight of the glass samples. Using CG as a raw material may contribute to the sustainability of the glass industry and positively impact the environment by reducing energy demand and the extraction of new raw materials from nature, ultimately reducing overall emissions and environmental footprint. Additionally, as we will show, these CG-derived materials may provide a platform for researching and developing new glasses and glass-ceramics for several applications.

2. Materials and methods

The weight of the compounds mixed to produce each sample is shown in Table 1, where the sample names refer to the %mol of CaF_2 . The CG, sourced from photovoltaic panels previously studied [20], was fragmented into particles approximately 5–10 mm in length. The reagents added to the mix were CaF_2 and Na_2CO_3 , both from Sigma-Aldrich with 99.0% purity. To keep the ratio $\text{SiO}_2/\text{Na}_2\text{O}$ approximately constant through all the samples, Na_2CO_3 concentration was adjusted accordingly. The reagents were mixed with the CG in a platinum crucible and heated in a furnace, following a heating ramp consisting of 40 minutes at 200°C , 60 minutes at 500°C , 90 minutes at 800°C , and 120 minutes at 1200°C . After this stage, the molten glass was poured into a stainless steel mold and rapidly transferred to a second furnace maintained at 480°C , where it was kept for about 12 hours to relieve internal stresses. Upon cooling to room temperature, the samples

Sample	Cover-glass (g)	CaF ₂ (g)	Na ₂ CO ₃ (g)	Total (g)
CgCAF05	13.00	1.00	1.94	15.94
CgCAF12	12.25	2.45	1.83	16.53
CgCAF15	11.80	3.00	1.76	16.56
CgCAF18	11.30	3.50	1.69	16.49
CgCAF20	10.90	4.00	1.63	16.53

Table 1: Mass of each sample prepared in this work

were removed from the mold. Figure 1 shows a photo of the obtained samples, which were cut, polished, or milled for the analyses.



Figure 1: Samples investigated in this work, as prepared, after removing from the mold.

The analytical techniques employed in this study encompass compositional, thermal, structural, and optical analyses. X-ray fluorescence (XRF) was used to determine the chemical composition of the samples. The analysis was performed on fused beads, and loss-on-ignition analysis was carried out to account for volatile content up to 1000 °C (Panalytical - Axios). Differential thermal analysis (DTA) was performed in the temperature range of 50°C to 900°C, using a heating rate of 10°C/min under a synthetic air atmosphere with a flow rate of 50 mL/min (TA Instruments – SDT Q600). The density of the samples was obtained using Archimedes’ principle with distilled water at room temperature. Mass measurements were performed with an analytical balance with a precision of ± 0.1 mg (Kern ABT - 120-5DM).

Structural characterization was performed by X-ray diffraction (XRD) was carried out on powdered samples. The analysis was performed using CuK α radiation ($\lambda = 1.5418$ Å) at 40 kV and 15 mA, with a scanning rate of 5°/min, step size of 0.02°, and a 2θ range from 5° to 80° (Rigaku - Miniflex 600). In situ XRD analysis was performed on powdered material to evaluate the temperature-dependent structural evolution. The measurements were conducted under air in the Bragg–Brentano geometry, using a 25°C step size from 500 °C to 950 °C, over a 2θ range of 15–60°, with a 0.016°C step size

and a counting time of 0.5 s/step. The powdered samples were placed in a platinum-lined corundum sample holder (Anton Paar - HTK1200N furnace with LynxEye detector).

Optical characterization involved Raman spectroscopy, UV-Vis-NIR and spectroscopic ellipsometry analysis. The Raman spectra were collected in a Bruker-Senterra Raman microscope using a 532 nm laser at 20 mW, in the spectral range of 50–1542 cm^{-1} . A $\times 20$ objective lens was used for laser focusing, and the signal was integrated for 2 seconds. Ultraviolet-visible-infrared (UV-Vis-Nir) transmittance was measured in the spectral range of 190–3600 nm (Shimadzu - 3600i Plus), and the refractive index of the samples was determined by spectroscopic ellipsometry at an incidence angle of 55° (HORIBA - UVSEL Plus).

Next, the experimental results obtained are presented.

3. Results and discussion

Though the CG is expected to be low iron soda lime glass, and the reagents added are quite pure, the samples were submitted to XRF analysis to confirm their composition. These results are shown in table 2. Assuming

Compound	CG	CgCAF05	CgCAF12	CgCAF15	CgCAF18	CgCAF20
SiO ₂	72.62	62.90	58.22	56.62	54.18	52.51
CaO	9.35	7.63	7.59	7.35	7.11	6.88
Na ₂ O	12.48	17.62	16.12	15.28	15.19	15.15
MgO	4.46	3.81	3.55	3.44	3.29	3.19
Al ₂ O ₃	0.48	0.37	0.36	0.33	0.31	0.32
K ₂ O	0.32	0.26	0.26	0.22	0.24	0.24
CaF ₂ *	-	5.20	12.40	15.25	17.98	20.61

Table 2: Composition obtained by XRF expressed as a percentage (%mol). *CaF₂ concentration was estimated assuming that Ca concentration obtained by XRF is the sum of CaO (from Cg) plus CaF₂ (added).

the CG composition obtained from the XRF analysis and the weights shown in table 1, we can calculate the stoichiometric relations for CgCAF samples, which are very similar to those obtained experimentally by XRF. In this way, though Fluorine is well known to be volatile, these results corroborate the assumption that no significant mass was lost during the melting process. As

previously stated, we also aimed to keep the ratio $\text{SiO}_2/\text{Na}_2\text{O}$ constant, and this XRF analysis confirms that this ratio is ~ 3.5 for all samples.

Figure 2 presents the X-ray powder diffraction (XRPD) patterns for all glass samples analyzed in this study, where the dotted lines represent Lorentzian fits applied to the experimental data to support the subsequent discussion. The absence of sharp peaks in all patterns confirms the amor-

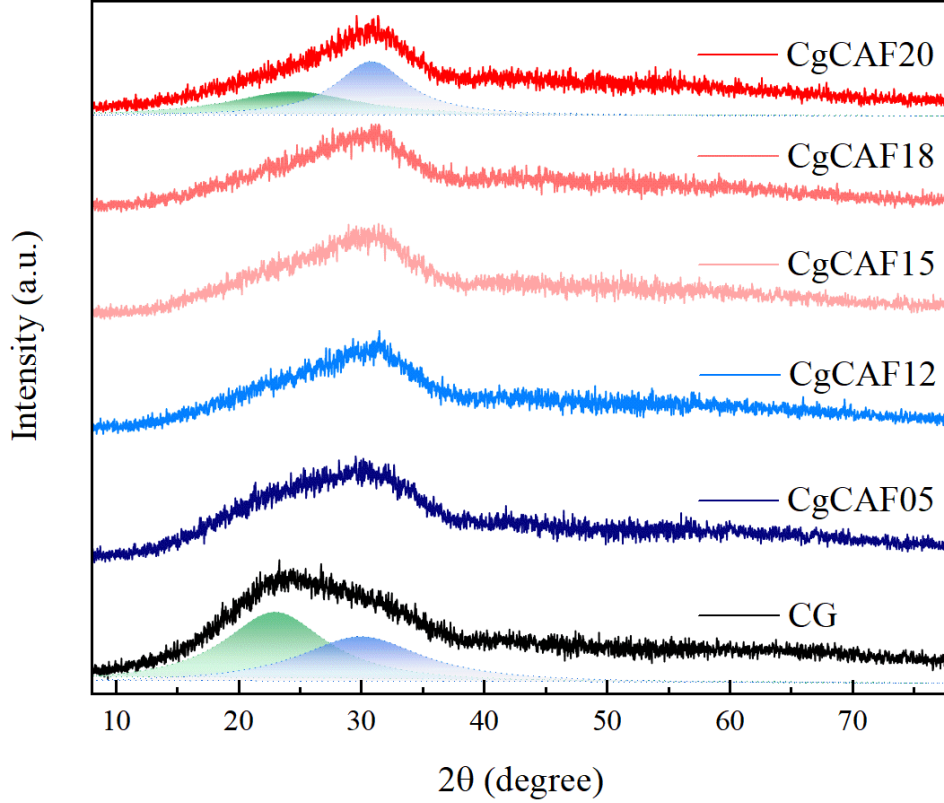


Figure 2: X-ray powder diffraction patterns.

phous nature of the samples, which is consistent with a glassy structural framework. These results agree with previously reported diffractograms for glasses and glass-ceramics of similar compositions [13, 21, 22]. Notably, the diffraction halos reveal the presence of two overlapping broad bands. To the CG, the predominant band is centered at approximately 22° , whereas for samples with increasing CaF_2 content, the dominant feature progressively shifts toward 30° . This behavior is likely associated with structural rearrangements driven by the incorporation of fluoride ions. As reported by

Iwamoto and Makino [23], fluoride ions in calcium fluorosilicate systems can engage in Si-F or Ca-F bonding. At lower CaF_2 concentrations, the formation of Si-F bonds is favored, whereas at higher concentrations, Ca-F interactions become more prominent. This transition is accompanied by a change in the fluoride coordination environment, from four-fold coordination, characteristic of a CaF_2 -type quasi-lattice, to six-fold coordination typical of a NaCl-type quasi-lattice. Notably, the NaCl-type structure possesses smaller average lattice parameters than the CaF_2 -type configuration. According to Bragg's law, a reduction in lattice spacing results in a shift of diffraction features toward higher 2θ angles. Nonetheless, confirmation of this hypothesis requires more comprehensive structural analyses, including advanced modeling approaches.

As demonstrated in table 2, CgCAF samples have a significantly lower proportion of SiO_2 compared to the CG as CaF_2 concentration increases. Figure 3, presents the mass density and refractive index at 628 nm as a function of CaF_2 concentration. The mass density of the samples increases linearly with the addition of CaF_2 , with an experimental uncertainty of $\pm 0.001 \text{ g/cm}^3$, which renders the associated error bars negligible in the graphical representation. This trend is consistent with the hypothesis of structural compaction, potentially arising from modifications in the local coordination environment of fluoride ions, as indicated by the shift of the amorphous halo observed in the XRD patterns. At the same time, the refractive index remained constant ($n \sim 1.52$) inside the error margins. Muniz et al. [13] have investigated sodium calcium silicate glasses containing amounts of CaF_2 similar to those in the present work, showing about the same mass density and a smaller refractive index (1.47).

Figure 4, presents the thermograms of all samples, including the CG, where the key events T_g (glass transition), T_x (onset of crystallization), and T_p (crystallization peak) are also indicated. However, in these experiments, T_x could not be identified for the CG, CgCAF05, and CgCAF12 samples. As one can see, in all CgCAF samples, it is possible to identify two crystallization peaks, a result widely observed in the literature on silicates containing CaF_2 [13, 16], as well as a significant reduction in the glass transition temperature ($\sim 50\text{-}90^\circ$). A summary of the characteristic temperatures identified for all samples is shown in table 3. It is essential to note the satisfactory glass stability ($T_x - T_g$) observed in these samples, suggesting a suitable working temperature that may enable these materials to be produced in different shapes and sizes. Though T_x could not be identified

An in situ high-temperature XRD study was performed in one sample

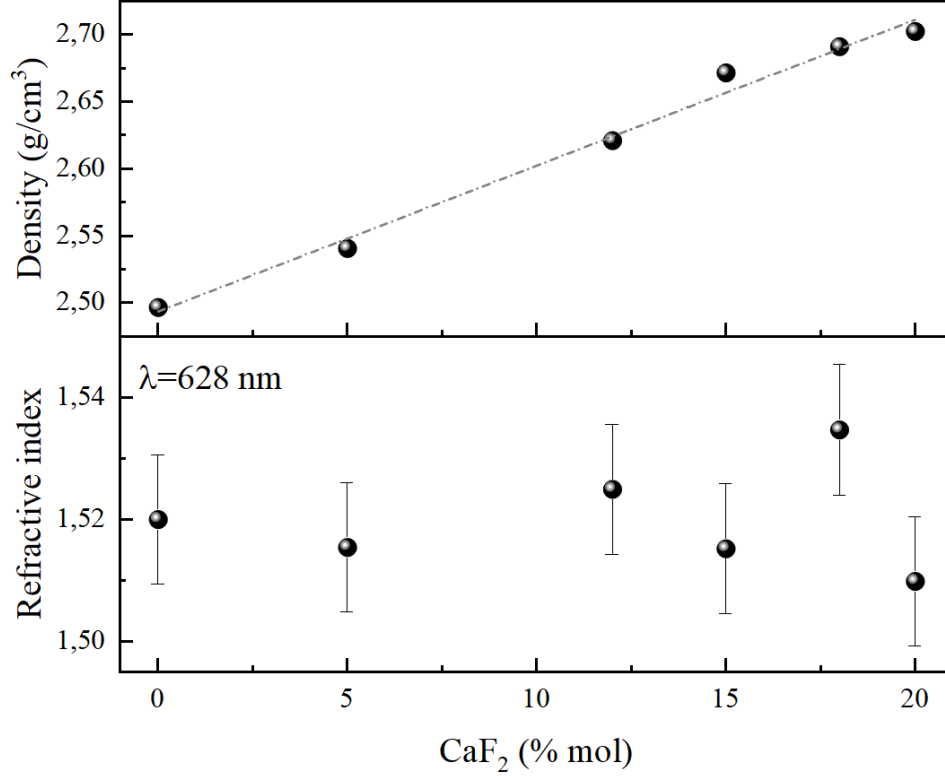


Figure 3: Mass density and refractive index at 628 nm of the samples as a function of CaF_2 concentration. Error bars are negligible for the density in this range.

(CgCAF12) to gain some insight into the crystallization characteristics of the material. These results are shown in figure 5.

Consistent with DTA measurements, a crystalline phase appears at 600°C. Nevertheless, we cannot identify this phase using the ICDD database. Additional work will be necessary to elucidate this point. The proportion of this unknown phase increases until 800°C and after decreases but is present in small amounts at 950°C. At 650°C we observe the crystallization of C3S (Ca_3SiO_5), which disappears at 800°C. The Combeite phase ($\text{Na}_4\text{Ca}_4\text{Si}_6\text{O}_{18}$) crystallizes around 675°C, and its proportion increases until 950°C to be finally the primary phase at HT. After this experiment, the XRD diagram collected at room temperature shows the presence of Combeite and a minimal amount of Akermanite. Some of these phases have been linked to intriguing features, such as antimicrobial activity [24]. This indicates that CG-derived

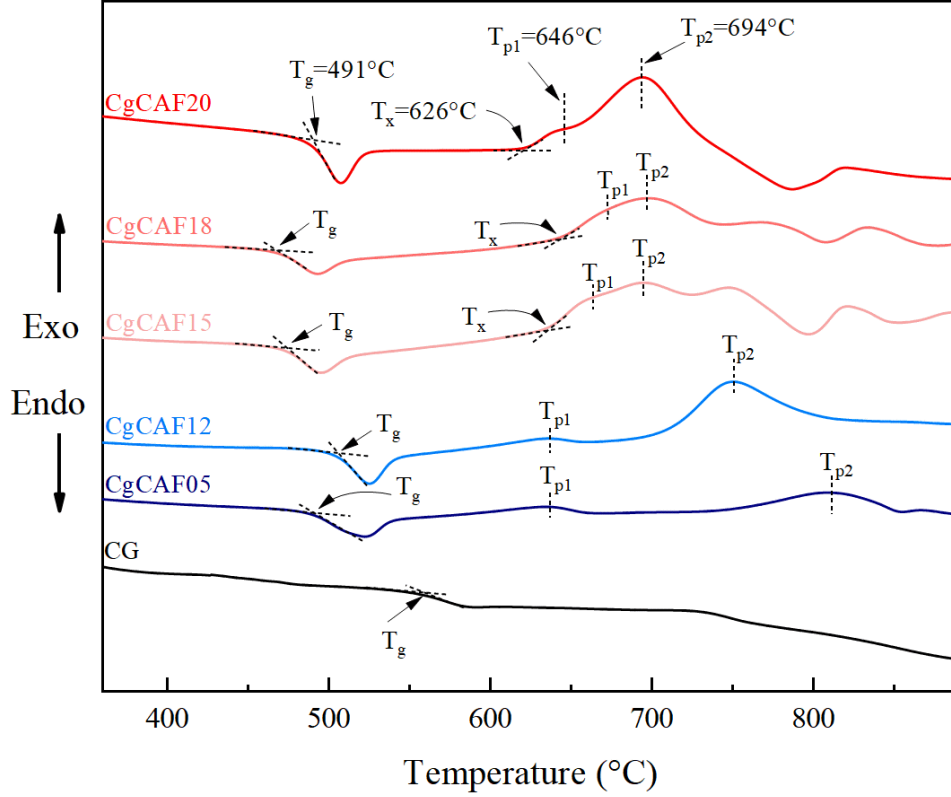


Figure 4: Differential thermal analysis of CG and CgCAF samples.

materials may also result in glass-ceramics with unique properties, which we will explore in future work.

Figure 6 shows the Raman spectra recorded for all samples, along with deconvolution using a multipeak Gaussian fit applied to the CgCAF05 sample (including the individual Gaussian components) as a representative example. Each Raman spectrum was fitted using 11 Gaussian components labeled (a to k) in the figure. This number was chosen based on the stability of the fitting process, as additional components did not significantly improve the quality of the fit. A weak band (g), located at approximately 870 cm^{-1} , could not be fitted for the CgCAF05 sample. The Raman scattering of the studied glasses is dominated by bands in the $550\text{--}750\text{ cm}^{-1}$ range (c, d, and e) and in the $900\text{--}1200\text{ cm}^{-1}$ region (h, i, j, and k). Raman spectroscopy has proven to be a powerful technique for the structural investigation of silicate glasses [25, 26, 27], although multiple overlapping bands pose a significant

Sample	T_g (°C)	T_x (°C)	$T_p(1)$ (°C)	$T_p(2)$ (°C)	$T_x - T_g$ (°C)
Cg	560	-	-	-	-
CgCAF05	491	-	636	812	-
CgCAF12	507	-	637	751	-
CgCAF15	475	636	664	695	161
CgCAF18	469	644	673	697	175
CgCAF20	491	626	646	694	135

Table 3: Thermal parameters of glass samples.

challenge for complete spectral interpretation.

The bands within the 900–1200 cm^{-1} range (h–i–j–k) are attributed to the symmetric stretching vibrations of Si–O bonds in various $[\text{SiO}_4]$ tetrahedral units, commonly referred to as Q^n bands (where $n = 0$ to 4), with n denoting the number of bridging oxygens per tetrahedron [28, 27]. It is well established that the band near 1100 cm^{-1} , associated with the Si–O vibration involving bridging oxygens, shifts to lower frequencies - or new bands emerge at lower frequency regions - due to the disruption of Si–O–Si linkages [29]. Furthermore, the primary determinant of Raman band frequency within this range is the force constant of the Si–NBO (non-bridging oxygen) bond. In silicate glasses containing CaF_2 , the substitution of oxygen atoms by fluorine distorts the silicon’s local electronic environment due to the higher electronegativity of fluorine. This distortion weakens the remaining Si–O bonds within the tetrahedra, leading to lower bond force constants and, consequently, lower associated vibrational frequencies [30]. This effect explains the slight “k” band shift with increasing CaF_2 concentration; this behavior was also observed by Muniz [31] for a similar composition glass.

On the other hand, the Si–F bond behaves similarly to the Si–O bond, and the stretching vibration of the Si–F bond in SiO_3F^- tetrahedra typically appears near 950 cm^{-1} in fluorine-containing silica glasses [30, 32]. Therefore, the formation of Si–F bonds may influence the frequencies of Si–O related vibrations and could account for the systematic increase in intensity observed for band “h” ($\sim 960 \text{ cm}^{-1}$) as CaF_2 content increases.

The bands in the 600 cm^{-1} region (c, d, and e) are assigned to symmetric vibrations of bridging oxygens (BO) in Si–O–Si linkages [28, 31]. In conventional soda-lime glasses, bands near 500 and 560 cm^{-1} are attributed to bending motions of Si–O–Si in highly polymerized tetrahedral structures (Q^4

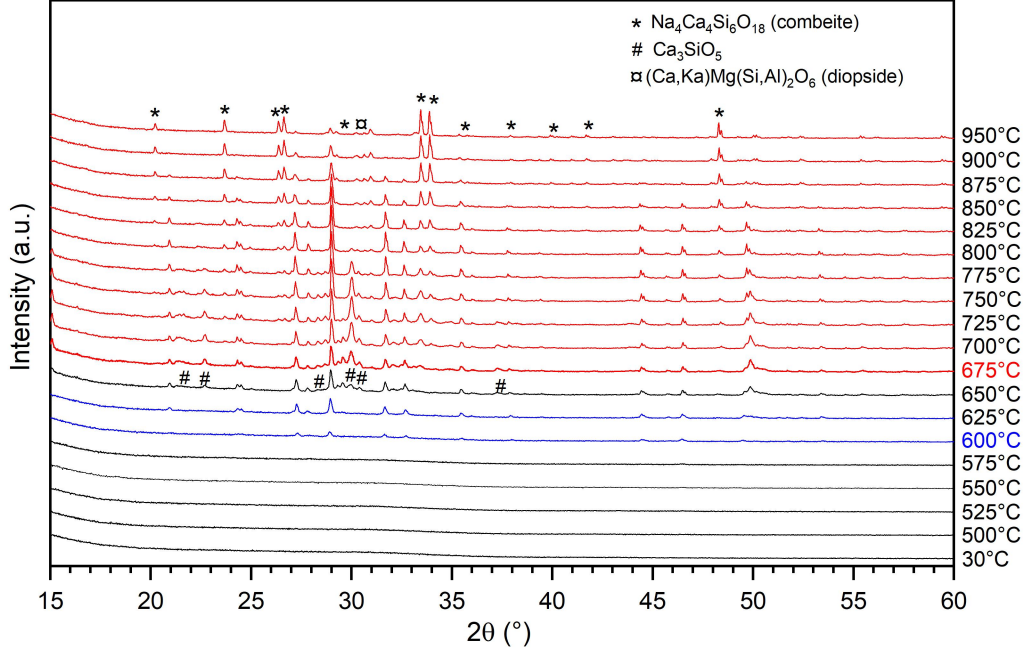


Figure 5: In situ XRD performed on the CgCAF12 samples.

and Q^3 species), while bands above 600 cm^{-1} are typically associated with Si-O bending in depolymerized $[\text{SiO}_4]$ tetrahedra (Q^2 species) [28, 33]. Although the Raman spectra of the intermediate samples (with CaF_2 contents ranging from 12.15 to 18 mol%) exhibit negligible variation among themselves, a notable shift of approximately 20 cm^{-1} is observed in the position of bands “e” and “k” when comparing the initial (CgCAF05) and final (CgCAF20) samples of the series. This spectral evolution indicates an increase in the fraction of non-bridging oxygens relative to total oxygens, suggesting a progressive depolymerization of the silica network with increasing CaF_2 content [13, 34, 35]. Such behavior implies significant structural modifications, including the possible formation of new Q^n species or phases, or a substantial reorganization within the silicate network.

The observed low-intensity Raman bands can also be identified. Band “a”, located near 350 cm^{-1} , is attributed to the vibrations of network-

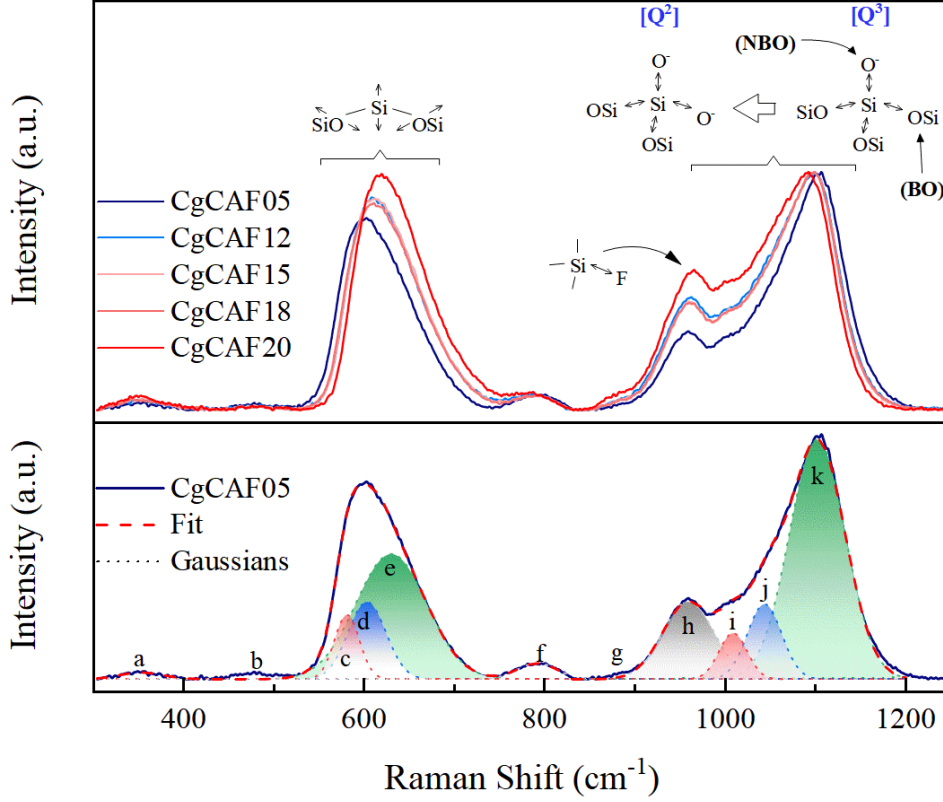


Figure 6: Raman spectra of CgCAF samples

modifying cations [31]. Although weak, its integrated area increases linearly with CaF_2 concentration. Band “f”, observed at 800 cm^{-1} and invariant concerning CaF_2 content, is assigned to Si–O stretching with dominant Si atom motion [36]. Symmetric stretching vibrations of Ca–F bonds are expected to appear around 485 cm^{-1} (band “b”) [30]. However, due to the highly ionic character of the Ca–F bond, Raman bands associated with these vibrations exhibit low intensity, and barely to no variation is observed as a function of CaF_2 content in the glass compositions studied.

Finally, samples of about 0.6 mm were used to measure the light transmittance in the range $190\text{--}3500 \text{ nm}$. These spectra are shown in Figure 7, demonstrating the overall high transmittance of the CgCAF samples. As shown in figure 3, the refractive index of these samples is $n \cong 1.5$, which translates to reflection losses of about 4% in each air-glass surface. As one can see, the transmittance remains near 90% from UV to the NIR, evidencing

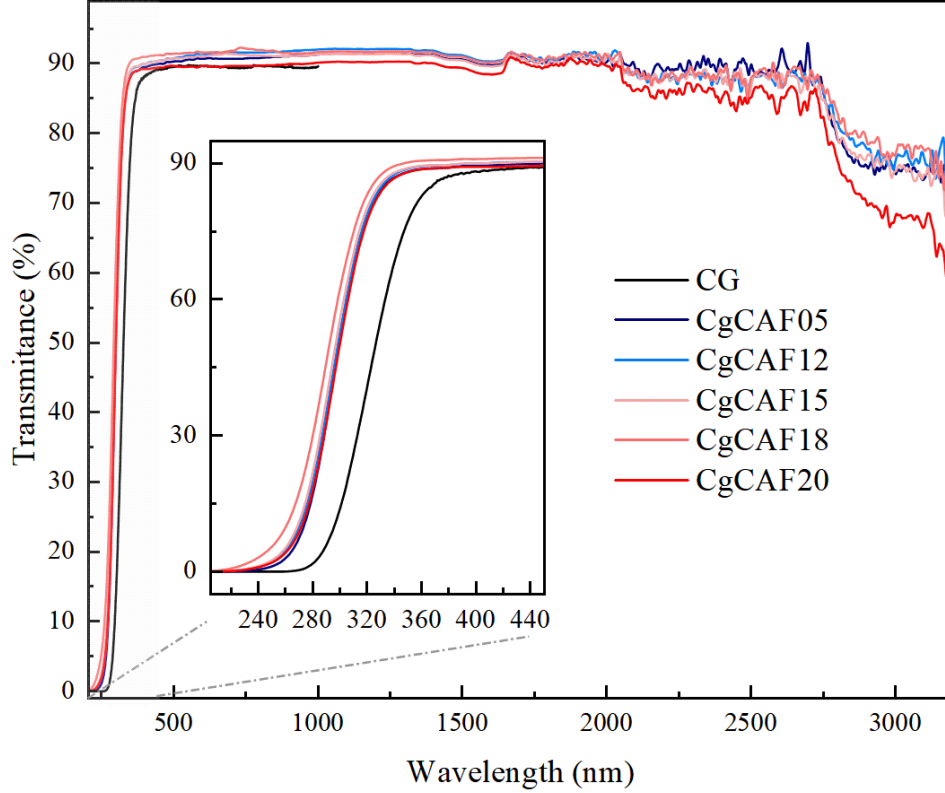


Figure 7: UV-VIS spectra

the high optical quality of the CgCAF samples in this range. As transmittance ($\sim 90\%$) plus reflection ($\sim 8\%$) accounts for about 98% of the incoming light, one can conclude that the absorption and scattering losses are pretty low in these samples. The inset in Figure 7 also highlights the wider transmittance window in the UV range of CgCAF samples compared to the original soda-lime glass, which may be associated with changes in the glass structure and could point to potential applications in UV-related technologies.

4. Conclusion

In this work, we have demonstrated the utilization of end-of-life cover glass from commercial solar panels to produce oxyfluoride glasses by incorporating CaF_2 . XRF analyses have proven that the final samples are free from contaminants, such as iron, that could introduce color to the material,

reducing its value and limiting its potential applications. This confirms that, thanks to the high purity and transparency of the soda-lime cover glass, we could use it to make up to 80% of the total weight of CgCAF glasses. In contrast, conventional flat glass production allows only a small proportion of the material to be recycled. Additionally, the melting temperature of the samples was about 1200°C, significantly lower than the melting temperature of soda-lime glass, which favors a reduced energy consumption and carbon emissions to produce CgCAF samples. The thermal analysis showed a 50-90°C reduction in T_g temperature relative to the soda-lime, the presence of at least two crystallization processes and a pretty good stability of the glass phase, demonstrated by $(T_x - T_g)$ values in the range 100-180°C. XRD confirmed the glassy nature of the samples and indicated a depolymerization process as the CaF_2 concentration increases, which is corroborated by mass density and Raman data. In situ XRD measurements in the CgCAF12 sample demonstrated the formation of combeite, diopside, and Ca_3SiO_5 triclinic phases, besides some unidentified peaks that require further studies. Finally, the UV-VIS-NIR transmittance demonstrated the good optical quality of all samples and the improved UV transmittance window compared to the original cover glass employed in this work. The ensemble of results shows that this family of materials can be explored as glass or be crystallized to produce glass-ceramics that may be tailored for different applications. Further studies should focus on understanding these materials' crystallization process and incorporating optically active ions. If these oxyfluoride glasses could be used at scale for some application, it could open up a path to reintroduce EOL cover-glass into the economy, improving its value and contributing to the industry's sustainability.

5. Acknowledgement

The authors thank CNPq (grants 409475/2021-1, 402473/2023-0 e 304060/2023-2) for the financial support.

References

- [1] D. D. F. D. Rio, B. K. Sovacool, A. M. Foley, S. Griffiths, M. Bazilian, J. Kim, D. Rooney, Decarbonizing the glass industry: A critical and systematic review of developments, sociotechnical systems and policy options (3 2022). doi:10.1016/j.rser.2021.111885.

- [2] M. Zier, P. Stenzel, L. Kotzur, D. Stolten, A review of decarbonization options for the glass industry (6 2021). doi:10.1016/j.ecmx.2021.100083.
- [3] J. H. Butler, P. D. Hooper, Glass Waste, 2nd Edition, Elsevier, 2019, pp. 307–322. doi:10.1016/B978-0-12-815060-3.00015-3.
URL <https://linkinghub.elsevier.com/retrieve/pii/B9780128150603000153>
- [4] B. Caudle, S. Taniguchi, T. T. Nguyen, S. Kataoka, Integrating carbon capture and utilization into the glass industry: Economic analysis of emissions reduction through co2 mineralization, Journal of Cleaner Production 416 (2023) 137846. doi:10.1016/j.jclepro.2023.137846.
URL <https://linkinghub.elsevier.com/retrieve/pii/S0959652623020048>
- [5] C. D. Westbrook, J. Bitting, M. Craglia, J. M. C. Azevedo, J. M. Cullen, Global material flow analysis of glass: From raw materials to end of life, Journal of Industrial Ecology 25 (2021) 333–343. doi:10.1111/jiec.13112.
URL <https://onlinelibrary.wiley.com/doi/10.1111/jiec.13112>
- [6] T. Bristogianni, F. Oikonomopoulou, Glass up-casting: a review on the current challenges in glass recycling and a novel approach for recycling “as-is” glass waste into volumetric glass components, Glass Structures & Engineering 8 (2023) 255–302. doi:10.1007/s40940-022-00206-9.
URL <https://link.springer.com/10.1007/s40940-022-00206-9>
- [7] M. P. Belançon, M. Sandrini, V. S. Zanuto, R. F. Muniz, Glassy materials for silicon-based solar panels: Present and future, Journal of Non-Crystalline Solids 619 (2023) 122548. doi:10.1016/j.jnoncrysol.2023.122548.
URL <https://linkinghub.elsevier.com/retrieve/pii/S0022309323004143>
- [8] X. Li, Q. Gu, Q. Wang, J. Luo, D. Liu, Y. Chang, Renewable energy in the mining industry: Status, opportunities and challenges, Energy Strategy Reviews 56 (2024) 101597. doi:<https://doi.org/10.1016/j.esr.2024.101597>.

URL <https://www.sciencedirect.com/science/article/pii/S2211467X24003067>

- [9] G. Gaustad, M. Krystofik, M. Bustamante, K. Badami, Circular economy strategies for mitigating critical material supply issues, *Resources, Conservation and Recycling* 135 (2018) 24–33. doi:10.1016/j.resconrec.2017.08.002.
- [10] D. Sica, O. Malandrino, S. Supino, M. Testa, M. C. Lucchetti, Management of end-of-life photovoltaic panels as a step towards a circular economy, *Renewable and Sustainable Energy Reviews* 82 (2018) 2934–2945. doi:10.1016/j.rser.2017.10.039.
URL <https://doi.org/10.1016/j.rser.2017.10.039>
- [11] T. Zink, R. Geyer, Material recycling and the myth of landfill diversion, *Journal of Industrial Ecology* 23 (2019) 541–548. doi:10.1111/jiec.12808.
- [12] R. F. Muniz, B. S. Greatti, M. Sandrini, M. P. Belançon, R. Valcarenghi, R. D. Bini, V. S. Zanuto, Glass Application in Solar Energy Technology, *Intechopen*, 2025. doi:10.5772/intechopen.1010177.
URL <http://dx.doi.org/10.5772/intechopen.1010177><https://www.intechopen.com/online-first/1218426>
- [13] R. F. Muniz, V. O. Soares, G. H. Montagnini, A. N. Medina, M. L. Baesso, Thermal, optical and structural properties of relatively depolymerized sodium calcium silicate glass and glass-ceramic containing CaF_2 , *Ceramics International* 47 (2021) 24966–24972. doi:10.1016/j.ceramint.2021.05.224.
URL <https://doi.org/10.1016/j.ceramint.2021.05.224>
- [14] R. F. Muniz, A. Steimacher, F. Pedrochi, V. S. Zanuto, L. M. Azevedo, J. H. Rohling, M. L. Baesso, A. N. Medina, Eu^{2+} - Nd^{3+} co-doped glasses for solar spectrum modification via $\text{UV}/\text{visible}$ to NIR downconversion, *Journal of Alloys and Compounds* 888 (2021) 161484. doi:10.1016/j.jallcom.2021.161484.
URL <https://doi.org/10.1016/j.jallcom.2021.161484>
- [15] J. Zheng, X. Xing, W. Liu, Z. Pang, R. Hu, Q. Xue, J. Wang, H. Zuo, An integrate study of the effects of CaF_2 on the viscous behavior and

- structure of cao-sio₂-mgo-al₂o₃-caf₂ blast-furnace slag, *Journal of Non-Crystalline Solids* 648 (2025) 123310. doi:10.1016/j.jnoncrysol.2024.123310.
- [16] M. Riaz, R. Zia, A. Mirza, T. Hussain, F. Bashir, S. Anjum, Synthesis, characterization of caf₂ doped silicate glass-ceramics, *Materials Science and Engineering: C* 75 (2017) 872–876. doi:10.1016/j.msec.2017.02.141.
URL <https://linkinghub.elsevier.com/retrieve/pii/S0928493116319798>
- [17] J. Xu, P. Chen, Effect of crystallization behavior and phase evolution on glass-ceramics derived from alumina silicate solid waste with addition high content caf₂, *Chemical Engineering Journal* 506 (2025) 159998. doi:10.1016/j.cej.2025.159998.
- [18] J. Laonamsai, P. Tasi, P. Wiwatrojanagul, M. Sriondee, T. Suriwong, P. Julphunthong, Synergistic effects of cuo and caf₂ additives in facilitating low-temperature tricalcium silicate formation and stabilization, *Results in Engineering* 26 (2025) 104620. doi:10.1016/j.rineng.2025.104620.
- [19] N. Pawlik, B. Szpikowska-Sroka, T. Goryczka, J. Pisarska, W. A. Pisarski, Structural and photoluminescence investigations of tb₃⁺/eu₃⁺-co-doped silicate sol-gel glass-ceramics containing caf₂ nanocrystals, *Materials* 14 (2021) 754. doi:10.3390/ma14040754.
- [20] M. P. Belançon, M. Sandrini, F. Tonholi, L. S. Herculano, G. S. Dias, Towards long term sustainability of c-Si solar panels: The environmental benefits of glass sheet recovery, *Renewable Energy Focus* 42 (2022) 206–210. doi:10.1016/j.ref.2022.06.009.
URL <https://linkinghub.elsevier.com/retrieve/pii/S1755008422000515>
- [21] R. P. F. de Almeida, C. Bocker, C. Rüssel, Size of caf₂ crystals precipitated from glasses in the na₂o/k₂o/cao/caf₂/al₂o₃/sio₂ system and percolation theory, *Chemistry of Materials* 20 (2008) 5916–5921. doi:10.1021/cm801426u.
URL <https://pubs.acs.org/doi/10.1021/cm801426u>

- [22] C. Rüssel, Nanocrystallization of CaF_2 from $\text{Na}_2\text{O}/\text{K}_2\text{O}/\text{CaO}/\text{CaF}_2/\text{Al}_2\text{O}_3/\text{SiO}_2$ glasses, *Chemistry of Materials* 17 (2005) 5843–5847. doi:10.1021/cm051430x. URL <https://pubs.acs.org/doi/10.1021/cm051430x>
- [23] N. Iwamoto, Y. Makino, A structural investigation of calcium fluorosilicate glasses, *Journal of Non-Crystalline Solids* 46 (1) (1981) 81–94. doi:10.1016/0022-3093(81)90076-4.
- [24] J. P. Caland, J. Baptista, G. C. Peiter, K. M. de Aguiar, H. Coelho-Júnior, J. P. Sinnecker, J. F. Felix, R. Schneider, Nanostructured glass-ceramic materials from glass waste with antimicrobial activity, *Molecules* 29 (7 2024). doi:10.3390/molecules29133212.
- [25] L. Vidal, E. Joussein, M. Colas, J. Cornette, J. Sanz, I. Sobrados, J. L. Gelet, J. Absi, S. Rossignol, Controlling the reactivity of silicate solutions: A ftir, raman and nmr study, *Colloids and Surfaces A: Physicochemical and Engineering Aspects* 503 (2016) 101–109. doi:10.1016/j.colsurfa.2016.05.039.
- [26] J. Gao, G. Wen, T. Huang, B. Bai, P. Tang, Q. Liu, Effect of slag-steel reaction on the structure and viscosity of CaO-SiO_2 -based mold flux during high-al steel casting, *Journal of Non-Crystalline Solids* 452 (2016) 119–124. doi:10.1016/j.jnoncrysol.2016.08.036. URL <https://linkinghub.elsevier.com/retrieve/pii/S0022309316303611>
- [27] H. Tian, Z. Wang, T. Zhao, C. Wang, A raman and multinuclear ^{29}Si , ^{27}Al , and ^{19}F nmr study on the structural roles of CaF_2 in $\text{SiO}_2\text{-CaO-Al}_2\text{O}_3$ -based welding fluxes, *Metallurgical and Materials Transactions B* 53 (2022) 232–241. doi:10.1007/s11663-021-02359-4. URL <https://link.springer.com/10.1007/s11663-021-02359-4>
- [28] A. K. Yadav, P. Singh, A review of the structures of oxide glasses by raman spectroscopy, *RSC Advances* 5 (2015) 67583–67609. doi:10.1039/c5ra13043c.
- [29] Y. Tsunawaki, N. Iwamoto, T. Hattori, A. Mitsuishi, Analysis of $\text{CaO}_2\text{-SiO}_2$ and $\text{CaO}_2\text{-SiO}_2\text{-CaF}_2$ glasses by raman spectroscopy, *Journal of Non-Crystalline Solids* 44 (2-3) (1981) 369–378. doi:10.1016/0022-3093(81)90039-9.

- [30] R. W. Luth, Raman spectroscopic study of the solubility mechanisms of f in glasses in the system $\text{cao-caf}_2\text{-sio}_2$, *American Mineralogist* 73 (3-4) (1988) 297–305.
- [31] R. Muniz, M. Baesso, F. Sato, A. Bento, J. Rohling, A. Medina, High pressure effect on the short-and intermediate-range structure of depolymerized soda lime silicate glass: Insights from micro-raman spectroscopy, *Vibrational Spectroscopy* 110 (2020) 103113. doi:10.1016/j.vibspec.2020.103113.
- [32] P. Dumas, J. Corset, Y. Levy, V. Neuman, Raman spectral characterization of pure and fluorine-doped vitreous silica material, *Journal of Raman spectroscopy* 13 (2) (1982) 134–138. doi:10.1002/jrs.1250130207.
- [33] M. Wang, J. CHeng, M. Li, F. He, Raman spectra of soda–lime–silicate glass doped with rare earth, *Physica B: Condensed Matter* 406 (20) (2011) 3865–3869. doi:10.1016/j.physb.2011.07.014.
- [34] A. Novatski, A. Steimacher, A. N. Medina, A. C. Bento, M. L. Baesso, L. H. C. Andrade, S. M. Lima, Y. Guyot, G. Boulon, Relations among nonbridging oxygen, optical properties, optical basicity, and color center formation in CaO-MgO aluminosilicate glasses, *Journal of Applied Physics* 104 (9) (nov 2008). doi:10.1063/1.3010306.
URL <https://pubs.aip.org/jap/article/104/9/094910/389590/Relations-among-nonbridging-oxygen-optical>
- [35] C. O’Shaughnessy, G. S. Henderson, H. W. Nesbitt, G. M. Bancroft, D. R. Neuville, The influence of modifier cations on the raman stretching modes of qn species in alkali silicate glasses, *Journal of the American Ceramic Society* 103 (2020) 3991–4001. doi:10.1111/jace.17081.
- [36] B. Boizot, S. Agnello, B. Reynard, R. Boscaino, G. Petite, Raman spectroscopy study of β -irradiated silica glass, *Journal of non-crystalline solids* 325 (1-3) (2003) 22–28. doi:10.1016/S0022-3093(03)00334-X.